

# Numerical study of quasiparticle lifetime in quantum dots

Alejandro M. F. Rivas and Eduardo R. Mucciolo

*Departamento de Física, Pontifícia Universidade Católica do Rio de Janeiro, CP 38071, 22452-970 Rio de Janeiro, Brazil*

Alex Kamenev

*Department of Physics, Technion, Haifa, 32000, Israel*

(September 25, 2001)

The decay rate of quasiparticles in quantum dots is studied through the real time calculation of the single-particle Green function in the self-consistent approximation. The method avoids exact diagonalization, transforming the problem into a system of coupled non-linear integral equations which may be solved iteratively. That allows us to study systems larger than previously treated in the literature. Our results for the inverse participation ratio of many-body states show that the threshold energy for the quasiparticle disintegration is  $E^* \sim \sqrt{g}\Delta$ . The delocalization transition is soft rather than sharp. Three different regimes as function of the effective interaction strength may be clearly identified at high energies.

## I. INTRODUCTION

Isolated quantum dots provide a unique opportunity to study the interplay between phase coherence, disorder, and electron-electron interaction effects in a confined geometry. These systems are realized experimentally in several forms; the best known example are the electron islands formed by the electrostatic lateral confinement of a two-dimensional electron gas in GaAs/GaAlAs heterostructures.<sup>1</sup> Among the important issues recently investigated is the lifetime of quasiparticle excitations that can be associated with the broadening of tunneling conductance peaks. In experiment reported in Ref. 2, for instance, few narrow peaks were observed above the Fermi energy, followed by a broad continuum. This result has initiated a theoretical discussion about the nature of the excited states in confined (but large) fermionic systems.

In this paper we study numerically the problem of quasiparticle decay rate in finite fermionic systems with chaotic single-particle dynamics. In most quantum dots, the presence of either disorder or complex boundaries lead to single-particle eigenstates displaying universal statistical properties. The universality takes place for states within the energy range of order  $g\Delta$  near the Fermi energy, where  $g \gg 1$  is the dimensionless conductance of the system (i.e., conductance in units  $e^2/\hbar$ ) and  $\Delta$  is the mean spacing between neighboring single-particle eigenenergies. The characteristic features of such states are level repulsion and spectral rigidity.<sup>3</sup> Moreover, the two-body (short-ranged) interaction matrix elements taken in the single-particle eigenbasis fluctuate according to Gaussian distribution whose standard deviation scales as  $1/g$ .<sup>4</sup>

Ref. 5 proposed to map the problem of quasiparticle lifetime onto an Anderson problem in the many-body Fock space. Upon such mapping, many-body states of

the noninteracting system are considered as “sites” of the Anderson lattice, while the interactions provide hopping between them. Since both the “on-site” energies and the hopping matrix elements are random (disorder dependent), one may expect a localization-delocalization transition to take place for certain values of the system parameters. For excitations with energy  $\varepsilon$  lower than the threshold energy  $E^*$ , the exact many-body states are “localized” in the single-particle basis. As a result, an excited quasiparticle evolves into a superposition of only few low-energy many-body eigenstates. The spectral function consists of a finite number of  $\delta$ -functional peaks and the quasiparticle lifetime is essentially infinite in this regime. At the energies above the delocalization threshold,  $\varepsilon > E^*$ , a large number of basis single-particle states contribute to a given exact many-body states. This eventually leads to spectral functions of the Breit-Wigner form whose width (inverse lifetime) may be evaluated employing the golden rule (GR).

To work out details of this crossover, Ref. 5 employed an approximate mapping of the many-body space of a fermionic system onto a Cayley tree (CT). Each generation of the CT corresponds to a set of many-body states with a given number of electron-hole pairs. Interactions (hopping) provide coupling between generations by exciting new electron-hole pairs. The advantage of such analogy is that the Anderson localization problem on the CT may be solved exactly.<sup>6,8</sup> Such solution indicates the existence of a sharp crossover at the energy  $E^* \sim \Delta\sqrt{g/\ln g}$ , where the participation ratio  $P$  jumps abruptly from a value close to unity in the localized phase ( $\varepsilon < E^*$ ) to infinity in the delocalized phase ( $\varepsilon > E^*$ ). The other important feature of the exact CT solution is the existence of a second characteristic energy  $E^{**} \sim \Delta\sqrt{g} > E^*$ . For excitation energies  $\varepsilon > E^{**}$ , the spectral density is of the Breit-Wigner form and the GR applies. On the other hand, for energies  $E^* < \varepsilon < E^{**}$ , the spectral density

consists of a very large number of narrow, but separate peaks (though the participation ratio is infinite).

The disadvantage of the CT mapping is that it is by no means exact. Indeed, it disregards potentially important effects such as existence of loops in the many-body space, correlations between on-site energies of different generations, and the fact that the actual number of accessible many-body states at a given energy is finite. Therefore, the predictions of the exact CT solution should be taken with a grain of salt. In fact, it is clear that no abrupt transition may happen, since the number of many-body states at the energy close to the critical one is exponentially large, but finite. As a result, the very existence of the transition, its quantitative features, and the characteristic energy scales are not firmly established by the CT picture. Several theoretical and numerical works<sup>7–15</sup> were devoted to clarification of these issues. One numerical study<sup>12</sup> claimed that for small systems the transition is absent and the quasiparticle lifetime decay can be well described by the GR. That conclusion does not apply to larger systems, where a breakdown of the GR is observed<sup>13</sup>. In large systems, one can explore a broader range of values of  $g$ , as well as higher excitation energies. Nevertheless, no signal of an abrupt transition was found. Essentially, all numerical work so far has relied on the exact diagonalization of the full many-body Hamiltonian (thus limited size Fock space), although under different assumptions regarding the structure of the two-body matrix elements.

Here we employ an alternative approach suggested by Levitov.<sup>16</sup> The method avoids matrix inversion or diagonalization and allows the investigation of large size systems. It is based on the calculation of the single-particle Green's function in real time. Adopting the self-consistent approximation for the self-energy, one can transform the problem into a non-linear integral equation which may be solved iteratively. The inverse participation ratio that measures the overlap between a one-particle state and the many-body eigenstates may be obtained directly from the long-time behavior of the Green's function. Our simulations involved up to 50 particles and 150 basis states (thus with filling factor 1/3; we deal with the spinless fermions for simplicity). The results confirm conclusions of Ref. 13, namely, that there is no sharp transition of the participation ratio (contrary to the case of an ideal CT). However, our estimate for the threshold energy at which quasiparticle states delocalize does not match the prediction of Ref. 5. Instead, our results are consistent with the scaling of the threshold energy as  $\Delta\sqrt{g}$ . We see no indications of other scalings such as those predicted in Ref. 14.

At the same time, our numerical data is consistent with the existence of the three different energy regimes, in agreement with Ref. 5. At small energies, single-particle states overlap with only a finite number of many-body states and quasiparticles do not decay. In the opposite limit, of large energy, the quasiparticles decay rapidly into the continuum of many-body states. The decay rate

follows closely the GR prediction. In the intermediate energy range, the quasiparticle is neither well defined (Fock-space localized), nor short lived, and GR does not apply.

This paper is organized as follows. In Sec. II we formulate the method used in the numerical simulations. The results are presented in Sec. III. Discussion and conclusions are left to Sec. IV.

## II. REAL-TIME GREEN'S FUNCTION APPROACH

The Hamiltonian of an isolated quantum dot with  $N$  spinless electrons may be separated into two parts,

$$H = H_0 + H_1, \quad (1)$$

where  $H_0$  contains one-body terms, such as the kinetic energy and the background potential, and  $H_1$  represents the two-body interactions. We denote  $\varepsilon_j$  and  $\phi_j(x)$  the single-particle eigenvalues and eigenfunctions of  $H_0$ , respectively. In this eigenbasis, one may write

$$H_0 = \sum_j \varepsilon_j c_j^\dagger c_j \quad (2)$$

and

$$H_1 = \sum_{j < k, m < l} V_{jk}^{lm} c_m^\dagger c_l^\dagger c_j c_k, \quad (3)$$

where the fermionic operators  $c_j$  and  $c_j^\dagger$  are, respectively, annihilation and creation operators of an electron on the state  $j$ . The interaction matrix elements are given by

$$V_{jk}^{lm} = \int dx \int dx' \phi_m^*(x) \phi_l^*(x') V(x - x') \phi_k(x) \phi_j(x'). \quad (4)$$

Below, we consider the case of short-range interactions of the form

$$V(x) = \lambda \Delta L^d \delta^{(d)}(x), \quad (5)$$

where  $L^d$  is the system volume and  $\lambda$  is the dimensionless interaction strength. Diagonal and off-diagonal matrix elements of the interaction have distinct statistical properties.<sup>5</sup> The diagonal ones,

$$V_{jk}^{jk} = V_{jk}^{kj} = \lambda \Delta L^d \int dx |\phi_k(x)|^2 |\phi_j(x)|^2, \quad (6)$$

have non-zero average value,  $\overline{V_{jk}^{jk}} \sim \lambda \Delta$ , while fluctuations around this mean value are small as  $g^{-1}$ . On the other hand the off-diagonal matrix elements

$$V_{jk}^{lm} = \lambda \Delta L^d \int dx \phi_m^*(x) \phi_l^*(x) \phi_k(x) \phi_j(x) \quad (7)$$

are zero in average,  $\overline{V_{jk}^{lm}} = 0$ , while their typical value is  $|\overline{V_{jk}^{lm}}| = \lambda\Delta/g$  for any choice of different  $j, k, l, m$  within the universal range  $\Delta g$ .<sup>4</sup>

In the absence of  $H_1$ , the ground state of the system is formed by the Slater determinant of the  $N$  lowest energy single particle eigenstates. That is, for eigenvalues arranged in ascending order, all states below and including the Fermi energy  $\varepsilon_F = \varepsilon_N$  are occupied and the remaining are empty. Excitations are formed by promoting one or more particles from the Fermi sea to the empty states above  $\varepsilon_F$ , leaving the holes behind. For instance, for an excited eigenstate formed by  $m$  particle-hole pairs,

$$|j_{2m}, \dots, j_{m+1}; j_m, \dots, j_1\rangle_0 = c_{j_{2m}}^\dagger c_{j_{m+1}}^\dagger \dots \times c_{j_m} \dots c_{j_1} |\text{FS}\rangle_0. \quad (8)$$

(Here, the subscript 0 is used to stress the absence of interactions.)

### A. The single-particle Green's function

Let us consider the (zero-temperature) time-ordered, single-particle Green's function ( $\hbar = 1$ ):

$$G_j(t) \equiv -i \langle \text{FS} | T \{ c_j(t) c_j^\dagger(0) \} | \text{FS} \rangle, \quad (9)$$

where  $|\text{FS}\rangle$  is the exact many-body ground state of the full Hamiltonian and  $T$  denotes the time ordering.

It is useful to review briefly the non-interacting case. The Green's function can then be written in the following form,

$$G_j^{(0)}(t) = \begin{cases} -i\theta(t) e^{-i\varepsilon_j t}, & \varepsilon_j > \varepsilon_F \\ i\theta(-t) e^{-i\varepsilon_j t}, & \varepsilon_j \leq \varepsilon_F \end{cases}, \quad (10)$$

where  $\theta(t)$  is the Heaviside step function. It is straightforward to show that

$$(i\partial_t - \varepsilon_j) G_j^{(0)}(t) = \delta(t), \quad (11)$$

with the initial conditions

$$G_j^{(0)}(0^+) = -i, \quad \varepsilon_j > \varepsilon_F^{(0)} \quad (12)$$

$$G_j^{(0)}(0^-) = i, \quad \varepsilon_j \leq \varepsilon_F^{(0)} \quad (13)$$

After the Fourier transform of Eq. (11), one finds

$$\tilde{G}_j^{(0)}(E) = \frac{1}{E - \varepsilon_j + i0^+ \text{sgn}(\varepsilon_j)}, \quad (14)$$

Thus,  $\tilde{G}_j^{(0)}(E)$  has a pole whose real part is exactly the  $j$ -th single-particle eigenenergy.

In the presence of interactions,  $H_1$ , the ground state is a superposition of a large number of Slater determinants. The same applies for the excited states, which are formed

by a superposition of many particle-hole states. Nevertheless, many aspects of the interactions, not related to the correlation effects, may be taken into account in the Hartree-Fock approximation. For instance, the diagonal part of  $H_1$  (related to matrix elements  $V_{jk}^{jk}$  and  $V_{jk}^{kj}$ ) can be incorporated into  $H_0$ , creating new sets of single-particle eigenstates  $\{\phi_j^{\text{HF}}\}$  and eigenenergies  $\{\varepsilon_j^{\text{HF}}\}$ , with the statistical properties similar to the noninteracting ones.<sup>18</sup> For our purposes, it is unnecessary to distinguish this new set from the original one and the Hartree-Fock superscript is dropped. By the same token, one may drop the diagonal elements. The off-diagonal ones are kept and are solely responsible for the finite lifetime of the quasiparticles.

The exact single-particle Green's function may be expanded perturbatively in ascending powers of  $\lambda$ . Through standard diagrammatic techniques, one arrives at the Dyson equation which generalizes Eq. (11) onto the interacting case,

$$(i\partial_t - \varepsilon_j) G_j(t) = \delta(t) + \int dt' \Sigma_j(t-t') G_j(t'). \quad (15)$$

The self-energy  $\Sigma_j(t)$  is the sum of all irreducible diagrams and contains the information about the structure of the excited states. In the frequency representation, one obtains

$$\tilde{G}_j(E) = \frac{1}{E - \varepsilon_j - \tilde{\Sigma}_j(E)}. \quad (16)$$

Thus, the self-energy shifts the pole of the Green's function with respect to the single-particle eigenenergy.

In the scheme proposed in Ref. 5, the self-energy involves only a limited class of diagrams. In order to motivate the approximation involved, let us view each excited many-body state formed by a Slater determinant of  $N$  eigenstates  $\{\phi_j\}$  as a site in Fock space. The two-body interaction term acts as a hopping matrix elements between sites, while the energy at each site is formed by a sum of the energies of the single-particle eigenstates present in the corresponding Slater determinant. The sites are considered as nearest neighbors when they differ only by one single-particle eigenstate. In fact, a more natural classification of the excited many-body states uses the number of particle and hole states.<sup>12</sup> Taking the noninteracting Fermi sea as a reference, we call a many-body state of class  $m$  ( $m > 0$ ) when it is formed by  $m$  particle and  $m - 1$  hole excitations. In Ref. 5, hopping between sites of the same class were not allowed; a site in class  $m$  could connect to all accessible sites in class  $m + 1$ , but to only one site in class  $m - 1$ . It is not difficult to see that these restrictions lead to the topology of a CT. It is important to notice that the coordination number of the tree at a given site depends on the site class and the excitation energy; eventually, for a sufficiently high class number, one runs out of single-particle states and further branching is interrupted. This fact was not properly taken into account in Ref. 5 when applying the results of Anderson localization problem.<sup>6</sup> As a result, while the Fock space

and the CT localization problems share a similar mathematical structure, they are not fully equivalent.

The same physics as in Ref. 5, with the proper branching number and on-site energy correlations, is fully encoded in the following self-consistent approximation for the self-energy,

$$\Sigma_j(t) = \sum_{klm} \left| V_{kl}^{jm} \right|^2 G_k(t) G_l(t) G_m(-t). \quad (17)$$

The resulting self-consistent equation for the Green's function is represented diagrammatically in Fig. (1). Equation (17) for the self-energy is the main approximation adopted in the present paper. We believe that it encompasses the essential physics of the model. In particular, it includes the "correct" CT structure with floating coordination number, as well as some of the possible loops in the many-body space. On the other hand, we have to stress that it is certainly not exact and some of the correlation effects are neglected by adopting Eq. (17).

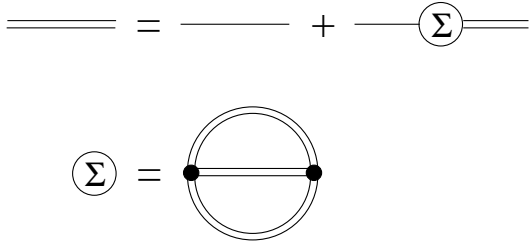


FIG. 1. Dyson equation and self-energy.

### B. The retardation ansatz

For our purposes, it is useful<sup>16</sup> to work with the real-time formulation, as in Eqs. (15) and (17), instead of the energy representation. In order to allow for an iterative solution of the non-linear coupled equations, we decompose the time-ordered Green's in particle-like and hole-like parts, depending on whether the index reference state  $j$  is above ( $\varepsilon_j > \varepsilon_F$ ) or below ( $\varepsilon_j \leq \varepsilon_F$ ) the Fermi energy, respectively. That is,

$$G_j(t) = \begin{cases} -i e^{-\varepsilon_j t} g_j(t), & \varepsilon_j > \varepsilon_F \\ i e^{-\varepsilon_j t} f_j(-t), & \varepsilon_j \leq \varepsilon_F \end{cases}. \quad (18)$$

It is now straightforward to obtain a set of integro-differential equations for the functions  $g_j(t)$  and  $f_j(t)$ . Let us, for convenience, assume  $\varepsilon_F = 0$ , such that  $j > 0$  corresponds to particle-like excitations, whereas  $j \leq 0$  corresponds to hole-like excitations.

Using Eq. (18) into Eqs. (15) and (17) for the case  $j > 0$ , we find that

$$\frac{dg_j(t)}{dt} = \delta(t) - \int dt' S_j(t-t') g_j(t') \quad (19)$$

with the kernel

$$S_j(t) = \sum_{\substack{k,l>0 \\ m\leq 0}} \left| V_{kl}^{jm} \right|^2 e^{it(\varepsilon_j - \varepsilon_k - \varepsilon_l + \varepsilon_m)} g_k(t) g_l(t) f_m(t). \quad (20)$$

Similarly, for  $j \leq 0$  we obtain

$$\frac{df_j(t)}{dt} = \delta(t) - \int dt' R_j(t-t') f_j(t') \quad (21)$$

with the kernel

$$R_j(t) = \sum_{\substack{k,l\leq 0 \\ m>0}} \left| V_{kl}^{jm} \right|^2 e^{-it(\varepsilon_j - \varepsilon_k - \varepsilon_l + \varepsilon_m)} f_k(t) f_l(t) g_m(t). \quad (22)$$

So far no additional approximation to Eq. (17) have been made. However, the self-consistent equations are still too complicated to be treated numerically. To proceed, we can explore the fact that the interactions are moderately weak ( $\lambda \sim 1$ ). Thus, the matrix elements  $V_{kl}^{jm}$  mix strongly only states that are nearly on shell, such that  $\delta\varepsilon = \varepsilon_j - \varepsilon_k - \varepsilon_l + \varepsilon_m$  is of order of  $\lambda\Delta/g$ . Since we are interested in, say, particle-like states with the typical energy  $\varepsilon \gg \delta\varepsilon$  we can disregard their admixture with the hole-like states and vice-versa. Neglecting such mixing amounts to looking for the solutions of the coupled integro-differential equations in the retarded form. (As matter of fact we disregard the difference between the retarded and time-ordered Green's functions for sufficiently large energies.) We thus set the initial conditions as stated above and substitute Eqs. (19) and (21) by

$$\frac{dg_j(t)}{dt} = - \int_0^t dt' S_j(t-t') g_j(t') \quad (23)$$

and

$$\frac{df_j(t)}{dt} = - \int_0^t dt' R_j(t-t') f_j(t'), \quad (24)$$

respectively, for  $t > 0$ . The computational advantage of the new equations over the original ones is obvious. For a given  $t$ , the integration runs over previous times only. Therefore, one can use the equations to iterate the initial condition forward in time to a certain given time  $t > 0$ . The error made in taking the retarded functions instead of the time-ordered one is measured by the parameter  $|V_{kl}^{jm}|/\varepsilon_j$ . In the region of the expected transition,  $\varepsilon_j \sim \Delta\sqrt{g}$ , this parameter is small. We believe therefore that the retardation ansatz, Eqs. (23) and (24), carries the same physical information as the self-consistent approximation, Eq. (17).

### C. Inverse participation ratio and real-time quasiparticle decay

Let us discuss characterization of the transition between the extended and localized states in the Fock space by the real-time single-particle Green's function method. Going back to Eq. (9), for  $t > 0$ , one finds

$$\begin{aligned} G_j(t) &= -i \sum_{\alpha} \langle 0 | c_j(t) | \alpha \rangle \langle \alpha | c_j^{\dagger}(0) | 0 \rangle \\ &= -i \sum_{\alpha} e^{it(E_0 - E_{\alpha})} \left| \langle 0 | c_j | \alpha \rangle \right|^2 \end{aligned} \quad (25)$$

where  $|\alpha\rangle$  denotes an eigenstate of the full Hamiltonian,  $H$ , with corresponding eigenenergy  $E_{\alpha}$ . As a result:

$$\begin{aligned} |G_j(t)|^2 &= \sum_{\alpha} |\langle 0 | c_j | \alpha \rangle|^4 + 2 \sum_{\alpha > \beta} |\langle 0 | c_j | \alpha \rangle|^2 |\langle 0 | c_j | \beta \rangle|^2 \\ &\quad \times \cos[(E_{\alpha} - E_{\beta})t]. \end{aligned} \quad (26)$$

Upon ensemble averaging, the oscillating term disappears. Indeed, since  $E_{\alpha} - E_{\beta}$  behaves as a random variable, at long enough times the average of the oscillating term in Eq. (26) rapidly goes to zero. One thus obtains

$$I_j \equiv \overline{|G_j(t)|^2}_{t \rightarrow \infty} = \sum_{\alpha} \overline{|\langle 0 | c_j | \alpha \rangle|^4}, \quad (27)$$

where  $I_j$  is the inverse participation ratio (IPR) for the Fock state  $c_j^{\dagger}|FS\rangle$ . In other words,  $P_j = 1/I_j$  is the number of many-body eigenstates that overlap with the quasiparticle state  $c_j^{\dagger}|FS\rangle$ . If a quasiparticle is localized in Fock space,  $P_j \approx 1$ , while in the extended case  $P_j \gg 1$ . Thus, for extended states  $I_j \rightarrow 0$  in the thermodynamic limit. In the later case one would expect the transition from localized and extended states to be marked by an abrupt jump in  $I_j$  as some parameter (the excitation energy,  $\varepsilon_j$ , interaction strength,  $\lambda$ , or the dimensionless conductance,  $g$ ) is varied.

### III. NUMERICAL SIMULATIONS

Equations (19) and (21) have obvious advantages over Eq. (15). Knowing  $g_j(t)$  and  $f_j(t)$  for all  $j$  and at all times  $t \leq t_0$  allows one to determine  $g_j(t_0 + \delta t)$  and  $f_j(t_0 + \delta t)$  by iteration, for sufficiently small  $\delta t$ . Thus, one can calculate the Green's function at any time starting from the initial conditions  $g_j(0) = f_j(0) = 1$  and  $\dot{g}_j(0) = \dot{f}_j(0) = 0$  (the latter follow from the integro-differential equations because the kernels are non-singular). Since no inversion or diagonalization is involved, one can treat rather large systems. In the present method the time cost increases with the number  $M$  of single-particle basis states. For the unconstrained summations in Eqs. (20) and (22) the time it takes to go through  $K$  iterations goes as  $K^2 M^4$  when  $N \lesssim M$ . Nevertheless, this time

can be substantially shorter than the diagonalization of a full many-body Hamiltonian matrix defined over the same  $M$  single-particle basis states.

The weakest point of the iterative calculation is the appearance of spurious numerical instabilities caused by the non-linearity of the coupled equations. However, we have found a good balance between  $K$ ,  $N$ , and  $g$  (for simplicity, we fixed  $\lambda = 1$ ). When the interactions are strong (small  $g$ ) and instabilities are more pronounced, the functions  $g_j(t)$  and  $f_j(t)$  decay faster and, despite  $\delta t$  being small (as compared to the Heisenberg time  $t_H = 1/\Delta$ ),  $K$  is not exceedingly large. If the interactions are weak (large  $g$ ), the decay is slow; we thus need to keep iterating up to  $t \gg t_H$  to achieve the stationary state implied by Eq. (27). However, in this case instabilities nearly do not occur and we can use larger  $\delta t$ . The number  $K$  was thus approximately the same for all values of  $g$ .

As pointed out in Ref. 13, one can simplify the numerical calculations without sacrificing the physics by restricting the number of connected states in Fock space. In the so-called layer model,<sup>11</sup> all non-diagonal matrix elements  $V_{jk}^{lm}$  except those with  $j + k = l + m$  are set to zero. This model provides a good approximation when the typical non-zero matrix element is much smaller than  $\Delta$ . For the layer model the number of total operations after  $K$  iterations decreases to  $K^2 M^3$ .

In the numerical simulations we also assume that the single-particle energy levels are random variables uniformly distributed in a sequence of intervals

$$\varepsilon_j \in [\Delta(j - 1/2); \Delta(j + 1/2)], \quad (28)$$

$j = 1, 2, \dots, M$ .<sup>13</sup> This has the clear advantage of providing some degree of level repulsion, consistent with Gaussian orthogonal (time-reversal symmetric) ensemble of random matrices, but without the inconvenience of a non-uniform level density. The number  $N$  of states with  $i \leq 0$  defines the number of particles present in the Fermi sea. The matrix elements of the interaction have to obey certain symmetries, namely,

$$\begin{aligned} V_{kl}^{jm} &= V_{jm}^{kl} \quad (\text{hermiticity}) \\ V_{kl}^{jm} &= -V_{kl}^{mj} = -V_{lk}^{jm} \quad (\text{fermionic character}). \end{aligned} \quad (29)$$

Each independent matrix element is chosen from a Gaussian distribution with zero average and  $\delta V = \Delta/g$  standard deviation. Notice that, after setting  $\lambda = 1$ , the interaction strength is controlled by the dimensionless conductance  $g \gg 1$ . The numerical algorithm solves the integro-differential equation by iteration (Cauchy problem), as in simulations of the time evolution of dynamical systems.

#### A. Results

Below we present the numerical results obtained for the layer model with 50 particles and 150 basis state and various values of  $g$ .

Figure 2 shows the averaged return probability  $|\overline{G_j(t)}|^2$  as a function of time  $t$  for various initial single-particle excited states  $j$  when  $g = 100$ . For comparison, we have also plotted the same quantity taken for a single realization (no averaging). Notice that in the latter case the return probability decays rapidly and then oscillates strongly. The averaging over different realizations suppresses such oscillations at large times, yielding a saturation at the inverse participation ratio value  $I_j$ . The higher the initial state energy  $\varepsilon_j$ , the lower the inverse participation ratio, showing an increasing coupling to the many-body eigenstates.

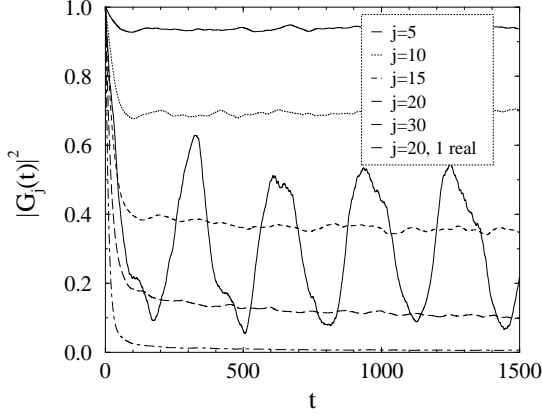


FIG. 2. Decay of the average return probability  $|\overline{G_j(t)}|^2$  for  $g = 100$  and various values of  $\varepsilon_j$ . The solid line corresponds to a single realization for  $j = 20$ . Time is given in units of Heisenberg time,  $t_H$ .

Figure 3 shows the local density of states (LDOS)  $\rho_j(E) = -\frac{1}{\pi} \text{Im} \tilde{G}_j(E)$  for a given realization of the system, but different values of  $j$ . This quantity characterizes the spreading of the single-particles states over the many-body eigenstates. One may observe three distinct regimes as the initial state energy is increased. At low  $j$  the initial state couples only to one or a few many-body eigenstates, thus corresponding to a state localized in Fock space. As the energy  $\varepsilon_j$  increases, the initial state begins to couple to a larger number of many-body eigenstates; the resulting LDOS shows a “fractal” structure, with multiple peaks located near zero energy. As  $\varepsilon_j$  increases further, the initial single-particle state overlaps to a much large number of many-body states, resulting in the merging of peaks and a rather broad LDOS. It is important to remark that upon ensemble averaging,  $\rho_j(E)$  always develops into a Breit-Wigner distribution (Lorentzian) regardless of the value of  $j$ . Only the width of the distribution depends on the initial state energy. Using the GR, one can estimate this width to be  $\Gamma_j = \frac{1}{3} \pi \Delta(j/g)^2$ .<sup>19</sup>

According to the CT model predictions,<sup>5</sup> the transition between localized and extended states in Fock space occurs at energy  $E^* \approx \Delta \sqrt{g/\ln g}$ . This implies a delocalization threshold at  $E^*/\Delta \approx 4.7$  for  $g = 100$ . However,

Fig. 3 suggests instead that quasiparticles survive for values of  $\varepsilon_j$  up to 10. In order to determine the position of the delocalization threshold, we have adopted the following criterion. A single-particle state is considered well defined when its coupling to many-body states is very weak and the corresponding participation number  $P_j$  should not exceed some small value (of the order of unity). Thus, we have estimated  $E^*$  as the energy necessary for  $P_j$  to reach a fixed value (for instance, 2). The resulting scaling behavior with respect to  $g$  is shown in Fig. 4 and is accurately described by  $E^* \sim \Delta \sqrt{g}$ . We also obtain the same scaling fixing  $P_j = 10$ . The difference between the square root scaling and the CT prediction is likely to be linked to the assumption of constant coordination number made in Ref. 5. As in the real situation, the branching number at each generation varies in the numerical simulations; eventually, it decreases abruptly when the number of particle-hole states is of the order of the number of particles in the system. As it was suggested in Ref. 8, taking into account the decreasing of the branching number with increasing the generation shifts the threshold energy to higher levels. This agrees with our numerical data.

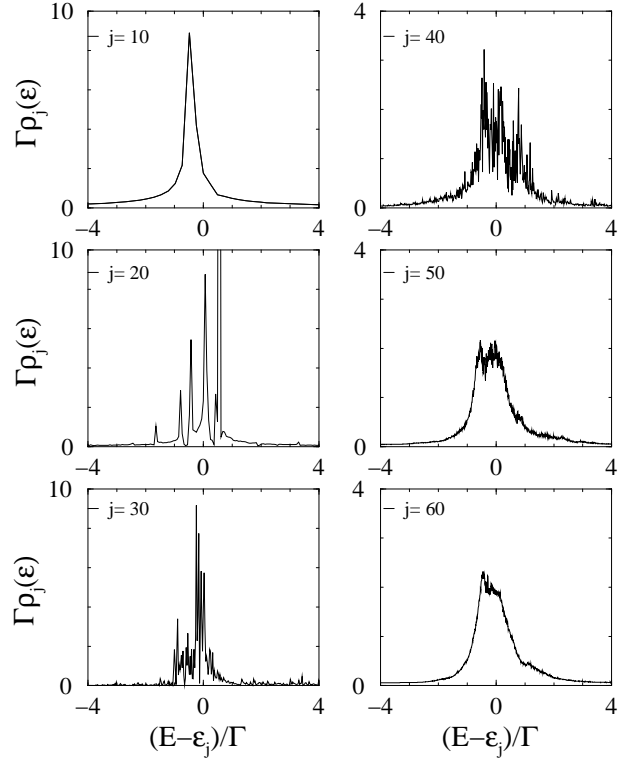


FIG. 3. Local density of states  $\rho_j(E) = -\frac{1}{\pi} \text{Im} \tilde{G}_j(E)$  for  $g = 100$  but different quasiparticles energies  $\varepsilon_j$ .  $\Gamma$  is the Breit-Wigner width expected from the golden rule prediction.

Following Ref. 12, we attempt to characterize the point of transition between the different regimes by plotting the average participation number  $P_j$  as a function of  $j$  (energy) for different values of  $g$ . The result is shown

in Fig. 5. The absence of cusps or shoulders in the graphs is a clear indication that no *sharp* transition between localized and extended states in Fock space takes place. Instead, the data is consistent with a continuous crossover, as previous exact diagonalization of small systems indicated.<sup>12</sup> We have checked that the same behavior holds for systems twice as large as well.

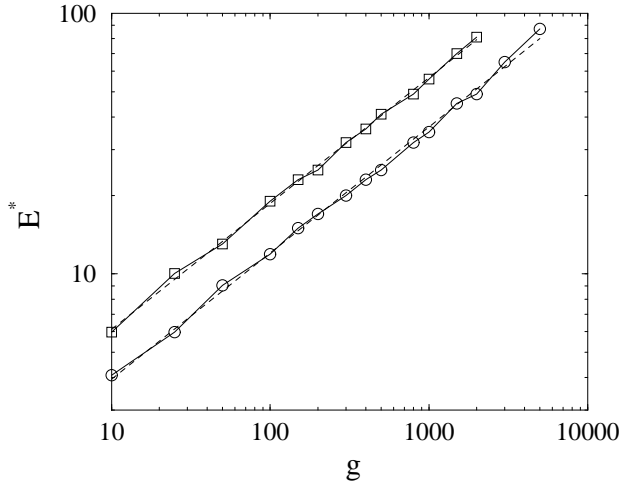


FIG. 4. Delocalization energy  $E^*$  for which  $P_j = 2$  (circles) or  $P_j = 10$  (squares) as a function of  $g$ . The dotted lines show the fits for  $E^* \sim \sqrt{g}$ .

In the fully delocalized, ergodic regime, quasiparticles couple to all energetically allowed many-body states. A way to characterize this regime is to fit the IPR  $I_j$  by the GR prediction, namely,  $I_j \approx \min(1, \delta/\Gamma)$ , where  $\delta$  is the mean many-body level spacing at a given energy. Since  $\delta/\Gamma \propto g^2$ ,<sup>19</sup> one expects a quadratic dependence of  $I_j$  with  $g$ . In Fig. 6 we present the IPR  $I_j$  as function of  $g$  for different values of  $j$ . It is clearly visible that there is a faster than quadratic increase in the IPR for high values of  $j$ . The quadratic behavior is restored as the interaction strength grows ( $g$  decreases). The failure of the GR prediction at large  $g$  occurs as one crosses a certain critical value, putting a given energy  $\varepsilon_j$  into the non-ergodic regime, namely,  $\varepsilon_j < E^{**}(g)$ . Although less pronounced, a similar behavior was observed for smaller systems in Ref. 13.

While Fig. 6 yields some information about the region where the IPR deviates from the GR prediction, it does not make clear where exactly ergodicity is broken. To quantify that Leyronas *et al.*<sup>15</sup> introduced a rescaled form of the IPR,  $F = -y \ln I_j$ , where  $x = (\varepsilon/g\Delta) \ln g$  is the rescaled dimensionless conductance and  $y = g(\Delta/\varepsilon)^{3/2}$  is the rescaling factor.<sup>11</sup> This quantity has the advantage of illustrating both extreme situations of localized and ergodic (delocalized) regimes in a much clearer way than  $I_j$  itself. For  $x < 1$  states are localized in Fock space and one can expand  $F$  in powers of  $x$  for a fixed  $\varepsilon_j$ ; Ref. 14 argues that the transition to the ergodic regime occurs for values of the parameter  $x \approx 1$ . In fact, at  $x \gg 1$ , the

small- $x$  perturbation theory diverges and  $F$  is expected to follow a behavior that can be deduced from the GR.

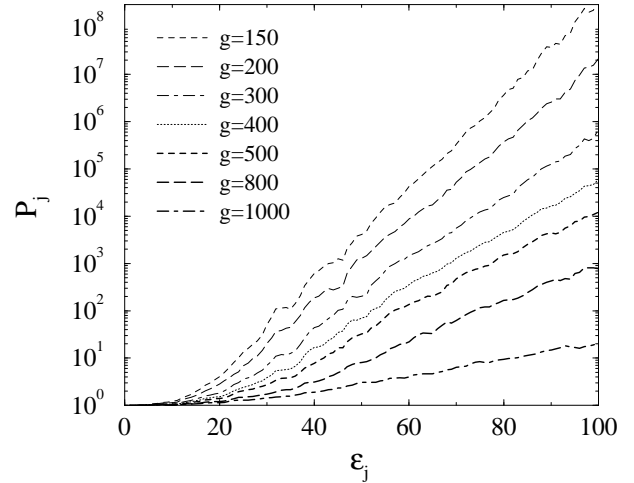


FIG. 5. Participation ratio as function of energy  $\varepsilon_j$  for different values of  $g$ .

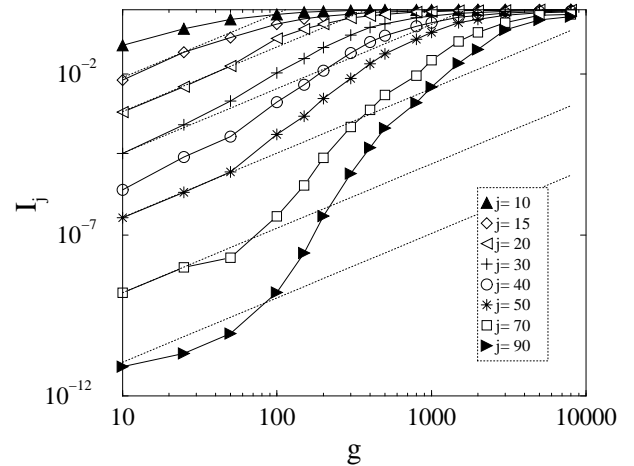


FIG. 6. Inverse participation ratio  $I_j$  as function of the dimensionless conductance  $g$  for different values of the energy  $\varepsilon_j$ . The dotted lines indicate the Fermi golden rule prediction.

In Fig. 7 we have plotted  $F$  as function of the rescaled dimensionless conductance  $x$ . Our results agree with those presented in Ref. 15 for small energies. However, as the energy is increased, three regimes (instead of two, as seen in Ref. 15) clearly appear. For large values of  $g$  or small  $x$  ( $x < 1$ ), where the perturbative calculation holds, the maximum of the function  $F$  shifts towards  $x = 0$ , as  $\varepsilon_j$  is increased. This may be interpreted as the appearance of higher than linear contributions to the perturbative expansion. Another notable behavior of the graphs at high  $\varepsilon_j$  is the absence of matching to the GR prediction for an extended range of  $x$  (when  $x > 1$ ). For instance, when  $j = 90$ , the GR prediction agrees with the numerical data only at  $x > 4$ . Thus, our results indicate existence of a range of values of  $g$  where there

is neither localization nor ergodicity (full delocalization). This range grows in size at higher energies.

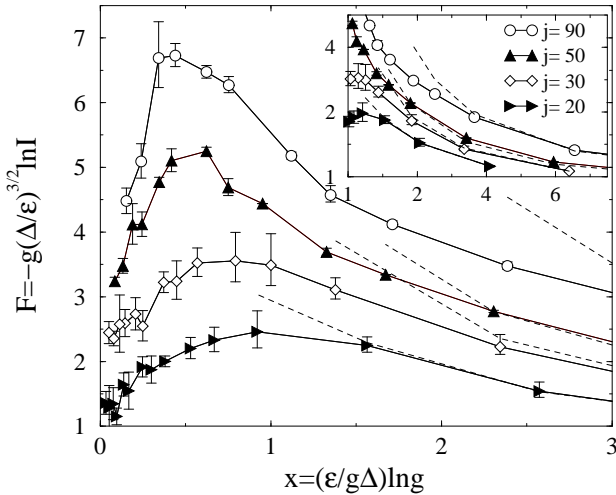


FIG. 7. Rescaled inverse participation ratio as function of the effective interaction strength  $x$  at different energies. The dashed lines are the golden rule prediction. The inset shows in the detail the large- $x$  behavior.

#### IV. DISCUSSION AND CONCLUSIONS

Using an approximate method in the time domain we have calculated the single-particle Green's function and extracted information about the quasiparticle decay rate. The method allows us to study larger systems than previously treated in the literature. At low energies our results are comparable to those obtained from direct diagonalization in small systems. At higher energies, however, we are able to identify three different regimes as function of the effective interaction strength. Furthermore, we have found that the delocalization threshold occurs at energies higher than the prediction of the CT mapping,  $\Delta\sqrt{g/\ln g}$ ; from our data, we estimate  $E^* \sim \Delta\sqrt{g}$ .

It is interesting to notice that a sequence of three different regimes in the absence of sharp transitions also occurs for quantum systems whose classical dynamics corresponds to the Komolgorov-Arnold-Moser (KAM) regime.<sup>11</sup> Indeed, drawing an analogy between the present problem and the KAM theorem of classical mechanics is very tempting. In that sense, the problem of a quasiparticle decay in a finite interacting system would be interpreted as a type of *soft*, interaction-induced crossover to chaos<sup>15</sup> rather than an abrupt transition for a particular value of  $\varepsilon_j$ .

Within this interpretation, the scaling behavior seen in the perturbative expansion around the localized state<sup>9</sup> corresponds to the theory of a regular classical system subjected to small symmetry breaking (potentially chaotic) perturbation. The radius of convergence of such theory breaks down at finite perturbation strength, indicating the onset of mixed dynamics (destruction of the

first phase space tori). Beyond the convergence radius, soft chaos is present, but there is no complete ergodicity yet. Indeed, our data for the IPR follow a similar behavior for intermediate values of the interaction strength  $g$ . The KAM analogy would be completed by connecting the onset of ergodicity in classical phase space (at sufficiently strong perturbations) to onset of the regime where the GR prediction for the IPR apply.

However, it is important to remark that we have not attempted to construct in any form a classical counterpart of the quantum many-body system.<sup>22</sup> Also, our approach does not give any information about the nature or the statistical fluctuations of the many-body excited states. Thus, we cannot confirm whether the quasiparticle decay problem and the KAM theorem are deeply related, or they just provide coincident regimes.

Recently, a few theoretical predictions have been made about the dynamics that governs the decaying process.<sup>20,21</sup> So far, no experimental or numerical simulations have corroborate these predictions. We plan to investigate this problem using the method here introduced.

#### V. ACKNOWLEDGMENTS

We are indebted to L. S. Levitov for suggesting the real-time approach used in this work. Stimulating discussions with B. L. Altshuler and C. H. Lewenkopf are acknowledged. A.M.F.R. and E.R.M. thank the Brazilian agencies CNPq, FAPERJ, and PRONEX for financial support. A.K. was partially supported by the BSF grant No. 9800338.

<sup>1</sup> L. P. Kouwenhoven *et al.*, in *Mesoscopic Electron Transport*, eds. L. L. Sohn, L. P. Kouwenhoven e G. Schön, Nato ASI Series E **345** (Kluvers, 1997).

<sup>2</sup> U. Sivan, F. P. Miliken, K. Milkove, S. Rishton, Y. Lee, J. M. Hong, V. Boegli, D. Kern, and M. deFranza, *Europhys. Lett.* **25**, 605 (1994).

<sup>3</sup> M. L. Mehta, *Random Matrices* (Academic Press, New York, 1991).

<sup>4</sup> A. D. Mirlin, *Phys. Rep.* **326**, 259 (2000).

<sup>5</sup> B. L. Altshuler, Y. Gefen, A. Kamenev, and L. S. Levitov, *Phys. Rev. Lett.* **78**, 2803 (1997).

<sup>6</sup> R. Abou-Chacra, P. W. Anderson, and D. J. Thouless, *J. Phys. C* **6**, 1734 (1973).

<sup>7</sup> P. Jacquod and D. L. Shepelyansky, *Phys. Rev. Lett.* **79**, 1837 (1997).

<sup>8</sup> A. D. Mirlin and Y. V. Fyodorov, *Phys. Rev. B* **56**, 13393 (1997).

<sup>9</sup> P. G. Silvestrov, *Phys. Rev. Lett.* **79**, 3994 (1997).

<sup>10</sup> R. Berkovits and Y. Avishai, *Phys. Rev. Lett.* **80**, 568 (1998).



- <sup>11</sup> B. Georgeot and D. L. Shepelyansky, Phys. Rev. Lett. **79**, 4365 (1997).
- <sup>12</sup> C. Mejía-Monasterio, J. Richert, T. Rupp, and H. A. Weidenmüller, Phys. Rev. Lett. **81**, 5189 (1998).
- <sup>13</sup> X. Leyronas, J. Tworzydło, and C. W. J. Beenakker, Phys. Rev. Lett. **82**, 4894 (1999).
- <sup>14</sup> P.G. Silvestrov, Phys. Rev. E **58**, 5629 (1998).
- <sup>15</sup> X. Leyronas, P. G. Silvestrov, and C. W. J. Beenakker, Phys. Rev. Lett. **84**, 3414 (2000).
- <sup>16</sup> L. S. Levitov, unpublished, (1997).
- <sup>17</sup> M. C. Gutzwiller, *Chaos in Classical and Quantum Mechanics* (Springer, New York, 1990).
- <sup>18</sup> S. Levit and D. Orgad, Phys. Rev. B **60**, 5549 (1999).
- <sup>19</sup> U. Sivan, Y. Imry, and A. G. Aronov, Europhys. Lett. **28**, 115 (1994).
- <sup>20</sup> V.V. Flambaum and F.M. Izrailev, Phys. Rev. E **64**, 026124 (2001).
- <sup>21</sup> P. G. Silvestrov, Phys. Rev. B **64**, 113309 (2001).
- <sup>22</sup> For an example where the classical analog of a toy model many-body system was obtained and studied in detail, see P. Leboeuf and M. Saraceno, J. Phys. A **23**, 1 (1990).